Biomass Conversion and Biorefinery (2025) 15:12931–12947
https://doi.org/10.1007/s13399-024-06006-1

ORIGINAL ARTICLE

Nanoporous carbons from hydrothermally pre-treated avocado waste: experimental design, hydrogen storage behavior, and energy distribution analysis

Lehlohonolo Mohale[1] · Jibril Abdulsalam[1] · Jean Mulopo[1]

Received: 29 May 2024 / Revised: 17 July 2024 / Accepted: 28 July 2024 / Published online: 20 August 2024

Abstract
Avocado waste, which includes the peel and seed, is a promising biomass source for highly porous materials crucial to establishing an economical and efficient hydrogen economy. Hydrothermally pre-treated avocado waste was explored as a precursor for biocarbon optimized for hydrogen storage, employing the design of experiment to vary activation temperature and impregnation ratio. The resulting optimized biocarbon, synthesized at 800 °C with a 1:3 impregnation ratio, exhibited appreciable hydrogen uptake at 77 K and 1 bar, surpassing some reported literature values. Notably, the optimized biocarbon (AC_{200}), hydrothermally pretreated at 200 °C, demonstrated a remarkable 3.07 wt% hydrogen uptake, attributed to its narrower micropores facilitating extensive adsorption. The study employed a modified Langmuir model incorporating homotattic patch approximation for a universal isotherm model, providing insights into the surface characteristics of the optimized biocarbon in terms of adsorption site availability and energy distribution. The modeling offers insight into the heterogeneous surface characteristics, specifically regarding the availability of adsorption sites, elucidating the distinct behavior exhibited by each optimized biocarbon.

Keywords Avocado waste · Biocarbon · Experimental design · Hydrogen storage · Universal adsorption isotherm model

Abbreviations

ANOVA	Analysis of variance
BET	Brunauer-Emmett-Teller
CCD	Central composite design
DoE	Design of experiment
EDF	Energy distribution function
EDX	Energy dispersive X-ray analysis
FTIR	Fourier transform infrared
HCl	Hydrochloric acid
HPA	Homotattic patch approximation
HTC	Hydrothermal carbonization
KOH	Potassium hydroxide
NLDFT	Non-local density functional theory
PSD	Pore size distributions
PV	Pore volume
R^2	Coefficient of determination
RSM	Response surface methodology
SA	Surface area
SEM	Scanning electron microscopy
XRD	X-ray diffraction

✉ Jibril Abdulsalam
jibril.abdulsalam@wits.ac.za; jibabdulsalam@gmail.com

[1] School of Chemical and Metallurgical Engineering, Faculty of Engineering and the Built Environment, University of the Witwatersrand, WITS 2050, Johannesburg, South Africa

1 Introduction

Sustainable energy development driven through shrewd energy policies can fortify the economy and improve social welfare. At the same time, the population's safety and security are strengthened, and the environment is conserved through pollution reduction [1]. Energy is crucial for the growth and long-term viability of any economy. It drives manufacturing, business, transportation of goods, and the delivery of services in the country. The energy industry plays a crucial role in driving both the economic and social growth of South Africa [2].

The global energy landscape is marked by a significant reliance on fossil fuels [3]. This dependence has resulted in significant progress in economic and industrial endeavors, albeit at the expense of significant environmental deterioration. Fulfilling the current energy needs entails guaranteeing

a consistent and dependable energy supply and tackling the environmental consequences of energy generation and usage. This necessitates developing and adopting cleaner, renewable energy sources that provide sustainable solutions.

Renewable energy sources, including solar, wind, hydro, geothermal, and biomass, have notable benefits compared to fossil fuels. They are abundant, environmentally friendly, and have minimal greenhouse gas emissions during operation [4]. Incorporating renewable energy sources into the worldwide energy portfolio is essential for diminishing reliance on non-renewable resources, decreasing greenhouse gas release, and alleviating climate change's impact.

Among the various renewable energy sources, biomass stands out due to its unique attributes and potential for widespread application [5]. Biomass energy is obtained from organic materials such as plant and animal waste, agricultural wastes, and forestry by-products [6]. Porous carbon materials derived from biomass have demonstrated significant potential. These materials, derived from biomass waste, possess large specific surface areas, tunable pore structures, and exceptional adsorption capabilities, making them suitable for hydrogen storage applications [5].

Hydrogen, as a clean energy carrier, has the potential to play a significant role in the transition to a sustainable energy future. Hydrogen is a cleaner and safer option with enormous energy potential. Hydrogen can be generated from renewable energy sources (such as solar, wind, and biomass) and converted to power in fuel cells, emitting just water and no greenhouse gases or other pollutants [3]. However, the absence of affordable storage options hinders the widespread adoption of hydrogen. This has a lot to do with the low density of hydrogen. Several other solutions for using hydrogen as a fuel are currently being explored. Hydrogen storage in adsorbent materials is a promising option. Adsorbents for this purpose must have extremely specific attributes depending on the temperature and physical state of storage in which they will be used.

Activated carbons are viable adsorbents for hydrogen storage due to their low cost, large surface area, and ease of synthesis [7]. Pyrolysis of a carbonaceous feedstock produces char with a basic pore structure, which is then activated chemically or physically to increase porosity. Over the past decade, porous carbon materials derived from biomass waste have seen diverse applications. Activated carbons from biomass waste have been widely studied as hydrogen storage material [8–12]. Ariharan et al. [13] demonstrated that biomass-derived porous carbon, through simple carbonization, is a superior material suitable for hydrogen storage and utilization in supercapacitors. Carbon products from biomass pine nutshells showed high surface area, large pore volume, and excellent electrochemical performance as supercapacitors [14]. These materials' highly developed porous structure makes them attractive for storage applications.

Studies on hydrogen storage utilizing activated carbon derived from biomass have demonstrated encouraging outcomes in terms of increased surface area, porosity, and storage capabilities. Research has concentrated on using several types of biomasses to synthesize activated carbons with remarkable hydrogen storage capacities. Activated carbons from pinecones, synthesized through dehydration at 453 K followed by KOH activation in varying ratios, exhibit significant hydrogen storage properties. The resulting activated dehydrated pinecone powders achieved a remarkable gravimetric capacity of 5.5 wt% at cryogenic temperature and 80 bar [12]. Porous carbon produced from food waste by hydrothermal carbonization at 220 °C and KOH activation at 800 °C resulted in a surface area of 2885 m^2/g and a pore volume of 1.93 cm^3/g. The hydrogen storage capacity increased from 4.53 to 6.15 wt% when the KOH/hydrochar ratio was increased from 2:1 to 4:1 [15].

Using KOH as an activating agent in synthesizing porous carbons from onion peel waste results in activated carbons with diverse morphologies and high surface areas. These activated carbons possess a sheet-like structure. The sample with the highest surface area of 3150 m^2/g and a pore volume of 1.64 cm^3/g also exhibited the highest hydrogen storage capacity, at 3.67 wt% at 77 K and 1 bar [16]. Porous-activated carbon from crushed Palimera sprout, carbonized and activated at 900 °C, showed a specific surface area of 2090 $m^2\ g^{-1}$ and a pore volume of 1.44 $cm^3\ g^{-1}$. These properties resulted in a gravimetric hydrogen storage capacity of 1.06 wt% at 298 K and 15 bar [17]. Activated porous carbons derived from bark and camellia shell using KOH and a mixed chemical pre-treatment showed significantly enhanced properties, with surface areas of 2849 $m^2\ g^{-1}$ and pore volumes of 1.08 $cm^3\ g^{-1}$. These carbons achieved notable hydrogen storage capacities of up to 3.01 wt% at 77 K and 1 bar and 0.85 wt% at room temperature [11]. Overall, the research status on biomass-based activated carbon for hydrogen storage shows promise for future practical use.

In 2019, global avocado production exceeded 7.18 million metric tonnes, increasing from 6.77 million in 2018. South Africa ranks as the world's 12th-largest producer of avocados [18]. Avocado's global output is predicted to increase between 2010 and 2030 as people become more health-conscious because of its health benefits [19]. As production output and demand increase, so does the waste generated during manufacturing and processing. Due to rigorous government requirements and a scarcity of landfill space, disposing of industrial waste has become increasingly challenging. In South Africa, regulations such as landfill levies are enforced to reduce the quantity of solid waste deposited in landfills. The increased expense of conveying a bulky and moist substance drives up the cost of landfilling even more. This gives an opportunity, especially considering the increased interest in the bio-economy, to develop value-added products such as

activated carbons from avocado waste to become adsorbents for hydrogen storage applications.

Our literature analysis indicates no studies have been published on using avocado waste as a feedstock for porous carbon for hydrogen storage. Previous studies have demonstrated that activated carbons derived from avocado waste, specifically the seed and peel, may effectively eliminate various emergent organic compounds [20], facilitate microextraction [21], remove phenol from water [22] and aqueous solutions [23], adsorb ammonia [24], eliminate dyes [25], and extract fluoride from groundwater [26].

The design of experiment (DoE) approach optimizes carbonization and activation processes by evaluating the interaction between multiple parameters [27], unlike the traditional one-variable-at-a-time method, which is time-consuming. Previous studies [27–30] have used DoE for optimizing activated carbon.

This study explores the potential of avocado waste as a feedstock for producing highly porous carbons for hydrogen storage, addressing the growing need for sustainable energy solutions and waste management. The study uses the design of experiment (DoE) method to optimize the activation process, evaluating multiple parameters simultaneously. By incorporating hydrothermal pre-treatment, the study seeks to enhance the efficiency and effectiveness of the activation processes. This study represents the first application of the DoE method to avocado waste for hydrogen storage, highlighting its innovative approach and contribution to sustainable energy development.

2 Materials and methods

2.1 Sample collection and preparation

Avocado waste, comprising peel and seed, was collected in an airtight sample bag from an avocado processing plant in Limpopo, South Africa, and was appropriately labeled for accurate identification. The avocado waste was dried under laboratory conditions for 48 h. After drying, the sample was ground and sieved to an average 100–200 µm particle size. The resulting powder was stored for characterization and hydrothermal carbonization.

2.2 Hydrothermal pre-treatment

Avocado waste underwent hydrothermal pre-treatment at varying temperatures to enhance its suitability as a precursor for activated carbon. A Berghof stirred pressure reactor, whose contents were stirred at 250 rpm, was used for hydrothermal pre-treatment. The biomass-to-water ratio was kept at 0.125, and the reaction temperature varied between 180 ℃, 200 ℃, and 220 ℃. Retention time was kept constant at 6 h (Masoumi et al., 2021). Following the reaction, the reactor was allowed to cool before the content was emptied onto a filter paper and allowed to separate the liquid and solid contents. The solid content was dried and stored for analysis. The hydrochars obtained were labeled HC_{180}, HC_{200}, and HC_{220}.

2.3 Activated biocarbon preparation

Activation was carried out using a suitable activating agent—potassium hydroxide (KOH)—and applied at varying impregnation ratios. The hydrochar (HC_{200}) with the highest surface area was selected as the precursor for the experiments in line with the experimental design. The activation temperatures varied from 700 to 900 °C, and the KOH-carbon precursor weight ratio varied from 1:1 to 3:1, respectively, to examine how they affected the properties of the resulting activated carbon. The material was cooled to room temperature under nitrogen gas flow after activation. The samples were washed using 1 M hydrochloric acid (HCl) and distilled water. The washed samples were dried at 105 °C in an oven overnight to obtain activated biocarbons.

2.4 Design of experiments (DoE)

The response surface methodology (RSM) has received considerable scholarly interest as a highly effective optimization technique. By utilizing the RSM method and a central composite design, the system was constructed to reduce the number of experiments [31, 32]. This statistical method facilitates the development and examination of empirical data, providing an efficient way to understand the correlation between analyzed parameters and system response, especially when used in conjunction with central composite design (CCD). RSM enables the examination of parameter interactions, resulting in cost and time savings [33]. The central composite was designed to fit a quadratic polynomial model with the fewest number of experiments, allowing for the evaluation of the interaction between process parameters and identifying the major component for response optimization. The chosen parameters, including activation temperature and impregnation ratio, as shown in Table 1, were systematically varied to evaluate their impact on the final activated carbon's characteristics.

These experimental parameters were combined, and the effect of their combination was evaluated using three response parameters: the BET surface area (S_{BET}), pore size, and hydrogen uptake at 77 K and 1 bar. The selected responses enabled the screening of materials in an efficient, high-throughput manner. The BET surface area is a dependable indicator of hydrogen absorption patterns among materials of the same group, providing a practical estimation of the number of adsorption sites [34, 35]. Prior

Table 1 Factors and levels of experimental central composite design

Factor	Units	Type	Coded low	Minimum value	Coded high	Maximum value	Mid-point
Activation temperature	°C	Numeric	−1	700	+1	900	800
Impregnation ratio		Numeric	−1	1	+1	3	2

studies have also shown a good correlation between gas sorption and the average pore size [27, 36–38]. As a result, the experimental design used BET surface, pore size, and hydrogen uptake as screening criteria to evaluate the performance of the synthesized carbon materials.

Design Expert Version 11.1.2.0 (Stat-Ease Inc., Minneapolis, USA) was used to evaluate the data. The quadratic polynomial model is often used to fit experimental data in RSM [31, 39]. The effect of factors was determined by fitting a quadratic polynomial model according to the equation (1):

$$y = \beta_0 + \sum_{i=1}^{k} \beta_i X_i + \sum_{i=1}^{k} \sum_{j=1}^{k} \beta_{ij} X_i X_j \sum_{i=1}^{k} \beta_{ii} X_i^2 + \varepsilon \quad (1)$$

where y represents the response, x is the process factors, βo denotes a constant term, β terms represent the model parameters, and ε represents the residual response variation [27]. By ascertaining numerical values for model parameters (β), the influence of each factor on the measured response was determined, as well as how these factors interacted to affect the response as a whole to ascertain the optimal process conditions [40].

2.5 Characterization methods

The proximate analysis of the avocado waste and hydrochars was conducted in accordance with the ISO 11722, 1171, and 562 standards [41], using a Leco TGA 701. The ultimate analysis of the sample (C, H, N, S, and O) was evaluated using LECO TruSpec CHN equipment and LECO Sulphur Analyzer, following ISO 12902 and ISO 19579 standards [42], respectively.

SEM/EDS analysis of the hydrochars and synthesized activated biocarbon was carried out using a Carl Zeiss Sigma Field Emission Scanning Electron Microscope (SEM) equipped with an Oxford X-act EDS detector. X-ray diffraction (XRD) was conducted using a Bruker D2 phaser equipped with Cu-Kα radiation (λ = 1.5405 Å), operating at 30 kV and 10 mA. Fourier transform infrared (FTIR) spectra were obtained using a PerkinElmer Spectrum 2 FTIR spectrometer. The surface area, pore volume, and pore size distribution were measured by analyzing nitrogen adsorption–desorption isotherms at 77 K using the Anton Paar Autosorb iQ instrument (Quantachrome Instruments, USA).

2.6 Hydrogen adsorption studies

The synthesized activated biocarbons produced were tested for hydrogen sorption at 77 K and 1 bar using Anton Paar Autosorb iQ. Adsorption tests were performed after degassing 0.1 g of each sample for 10 h at 200 °C [43]. Multiple samples synthesized under different conditions were tested to identify optimal parameters for enhanced hydrogen storage performance.

2.7 Modeling

The universal adsorption isotherm model developed by Ng et al. [44] was used to predict the adsorption behavior of the activated biocarbons. The model, a unified approach for the adsorption isotherm, is an improvement of previous adsorption models that could only accurately represent a particular region of adsorption but failed to predict other regions universally. The model combines three components: (i) homotattic patch approximation (HPA), (ii) updated Langmuir model, and (iii) fractional probability factor for the distribution of site energy sets. This universal model aims to simplify the process of adsorption on a complex and heterogeneous porous surface [44].

The heterogeneous surface of the adsorbent is represented by smaller homogeneous surfaces that are assumed to have the same energy level within each site. Each homogeneous surface was defined through the adsorption site energy distribution function (EDF). The probability of an adsorption site indicated the localized adsorption uptake within the monolayer. This depends on the type of pores in the layer. A fractional probability component was included to account for changes in the multi-layer formation. This factor indicates the proportion of the total surface covering or energy distribution of each pore size or adsorbate layer in the formation [44].

The assumption was that there would be just one molecule per adsorption site, and a homotattic patch approximation would be used. The adsorption capacity at a uniform patch/surface is presented in equation (2)

$$\theta(\varepsilon_j) = \frac{n_j}{s_j} \tag{2}$$

where n_j represents the number of molecules and s_j the local adsorption sites available. As a consequence, the total adsorption uptake available at an adsorbent surface is given in equation (3):

$$\theta_t = \frac{N_a}{S_0} = \sum_{j=1}^{\infty} \theta(\varepsilon)_j \tag{3}$$

where N_a represents the total number of adsorbed molecules and S_o the total number of available sites.

According to Ng et al. (2017), Type-VI isotherm energy distributions have four peaks, so four probability factors are used to express the energy distribution functions, $\alpha_1 + \alpha_2 + \alpha_3 + \alpha_4 = 1$. However, two terms are sufficient for a Type-IV isotherm as shown in equation (4).

$$\theta_t = \alpha_1\left[\frac{\left(\frac{p}{p_s}\exp\left(\frac{\varepsilon_{o1}}{\mathrm{RT}}\right)\right)^{\frac{\mathrm{RT}}{m1}}}{1+\left(\frac{p}{p_s}\exp\left(\frac{\varepsilon_{o1}}{\mathrm{RT}}\right)\right)^{\frac{\mathrm{RT}}{m1}}}\right] + \alpha_2\left[\frac{\left(\frac{p}{p_s}\exp\left(\frac{\varepsilon_{o2}}{\mathrm{RT}}\right)\right)^{\frac{\mathrm{RT}}{m2}}}{1+\left(\frac{p}{p_s}\exp\left(\frac{\varepsilon_{o2}}{\mathrm{RT}}\right)\right)^{\frac{\mathrm{RT}}{m2}}}\right]$$

$$+\alpha_3\left[\frac{\left(\frac{p}{p_s}\exp\left(\frac{\varepsilon_{o3}}{\mathrm{RT}}\right)\right)^{\frac{\mathrm{RT}}{m3}}}{1+\left(\frac{p}{p_s}\exp\left(\frac{\varepsilon_{o3}}{\mathrm{RT}}\right)\right)^{\frac{\mathrm{RT}}{m3}}}\right] + \alpha_4\left[\frac{\left(\frac{p}{p_s}\exp\left(\frac{\varepsilon_{o4}}{\mathrm{RT}}\right)\right)^{\frac{\mathrm{RT}}{m4}}}{1+\left(\frac{p}{p_s}\exp\left(\frac{\varepsilon_{o4}}{\mathrm{RT}}\right)\right)^{\frac{\mathrm{RT}}{m4}}}\right] \tag{4}$$

where θ_t is the total adsorption uptake, α the probability factor, and p_s is the saturation pressure at the maximum possible uptake by an adsorbent,

Equation 4 is an expanded form of Eq. 3, without the intermediate steps, to reflect the number of sets of adsorption sites available and their distributions in an isotherm. Two terms for Type-I to Type-V isotherms and four terms for Type-VI isotherms but less or more than four terms can be used for Type-VI isotherms considering the complexity of the multi-layer behavior. [44].

3 Results and discussion

3.1 Avocado waste characterization

Table 2 shows the results of the avocado waste proximate, ultimate, and total sulfur analysis. The results of proximate analysis for avocado waste show crucial properties that make them potential precursors of activated carbon. It has an 8.68% moisture and 12.95% fixed carbon. Low moisture content is generally preferred to enhance the efficiency of the carbonization process and improve the yield of activated carbon [45]. A high volatile matter content of 76.15% is beneficial as it promotes the formation of a more porous structure in the resulting char [46]. The low ash content of 2.22% is favorable as high ash content can impede the development of porous structures by blocking pores and reducing the available surface area for adsorption [45]. From the proximate analysis, it can be seen that avocado waste is a viable feedstock for synthesizing high-porous carbon materials. This is consistent with results from other biomass sources, strengthening the argument for using agricultural waste for sustainable carbon materials [47].

Table 2 Proximate, ultimate, and total sulfur analysis of the avocado waste sample

Analysis	Avocado waste
Proximate analysis (wt%)	
Moisture content	8.68
Volatile matter	76.15
Fixed carbon	12.95
Ash	2.22
Ultimate analysis (wt%)	
Carbon	43.69
Hydrogen	6.17
Nitrogen	1.10
Oxygen	49.04
Sulfur	0.00

The ultimate analysis of avocado waste material provides valuable insights into its elemental composition, which is crucial for understanding its potential applications. The results obtained from the ultimate analysis are shown in Table 2. According to the results, the avocado waste has a high percentage of carbon and oxygen and a low amount of hydrogen and nitrogen. This composition agrees with the high starch content in avocado seeds reported by Bressani et al. [48].

The carbon content of 43.69% observed in the avocado waste sample suggests its potential as a carbon-rich feedstock. The high carbon content shows the presence of organic carbonaceous materials in avocado waste, which can serve as precursors for carbonization processes [49]. Hydrogen storage in porous carbon materials relies on physisorption, where hydrogen molecules are attracted to and held onto the surface and pores of the carbon matrix [50]. The presence of nitrogen (1.1%) and oxygen (49.04%) in the avocado waste sample can enhance hydrogen adsorption by providing more surface sites and promoting polar interactions with hydrogen molecules [51]. The absence of sulfur in avocado waste is advantageous, as sulfur can lead to undesirable emissions or corrosion issues during thermochemical conversion processes. With zero sulfur content, avocado waste poses minimal environmental risks and can be processed without concerns about sulfur-related complications.

The supplemental material includes a detailed characterization of the hydrochars obtained from pre-treating the avocado waste at different temperatures (Table S1, Figs S1, and S2).

3.2 Impact of factors on the properties of avocado waste-derived biocarbon

RSM was used to study the effect of process factors on the adsorptive characteristics of avocado waste biocarbons. Table 3 presents the finalized experimental design and the corresponding measured results. The parameters investigated were activation temperature (A_{Temp}) and KOH weight ratio (K_{wr}). The measured responses included the BET surface area (S_{BET}), average pore size (PS), and hydrogen uptake at a temperature of 77 K and pressure up to 1 bar. The impact of temperature and chemical reagent weight ratio on the surface area, pore size, and hydrogen adsorption of synthesized activated biocarbons is explored in this section.

Table 3 Experimental design matrix and measured responses

Experimental number #	Experimental parameters		Measured responses		
	A_{Temp} (°C)	K_{wr}	S_{BET} (m^2/g)	PS (nm)	H_2 uptake (wt%)
1	800	2	1482.8	2.18	2.57
2	700	3	928.8	2.17	1.65
3	800	1	1201	2.23	1.84
4	700	2	518.9	5.36	1.38
5	900	1	450.15	6.04	1.32
6	800	1	1151.7	2.01	1.85
7	800	3	2329.8	2.3	2.91
8	900	2	510.5	2.75	1.42
9	900	3	533.614	2.85	1.49
10	800	3	2488.98	2.26	3.04
11	700	1	244.79	4.23	1.13

3.2.1 Impact of activation temperature on adsorptive properties of synthesized biocarbon

The adsorptive properties of the synthesized activated biocarbons as obtained from nitrogen and hydrogen adsorption at 77 K are summarized in Table 3. The influence of temperature on the properties of the activated samples can be observed from the results shown in Table 3 and Fig. 1. The results demonstrate that as the temperature increases, the surface area also increases. The largest surface area recorded was 2488.98 m^2/g at a temperature of 800 °C, corresponding to a larger hydrogen uptake. Multiple studies have shown that the temperature at which activation occurs substantially impacts the formation of the porous structure and is the most influential factor in the synthesis of activated carbon [52, 53]. As shown in Table 3 and Fig. 1A, the activation temperature caused an increase in surface area from 700 to 800 °C; however, it declined once the temperature surpassed 800 °C. Higher temperatures enhance the carbonization and gasification processes, leading to developed pore formations, which help increase the total surface area with a corresponding improvement in adsorption capacity [32, 52]. The study by Wang et al. [54] highlights the temperature-dependent evolution of surface area, providing insights into the nuanced mechanisms governing this phenomenon. While higher activation temperatures generally lead to increased surface area, maintaining balance is crucial. Excessive temperatures can

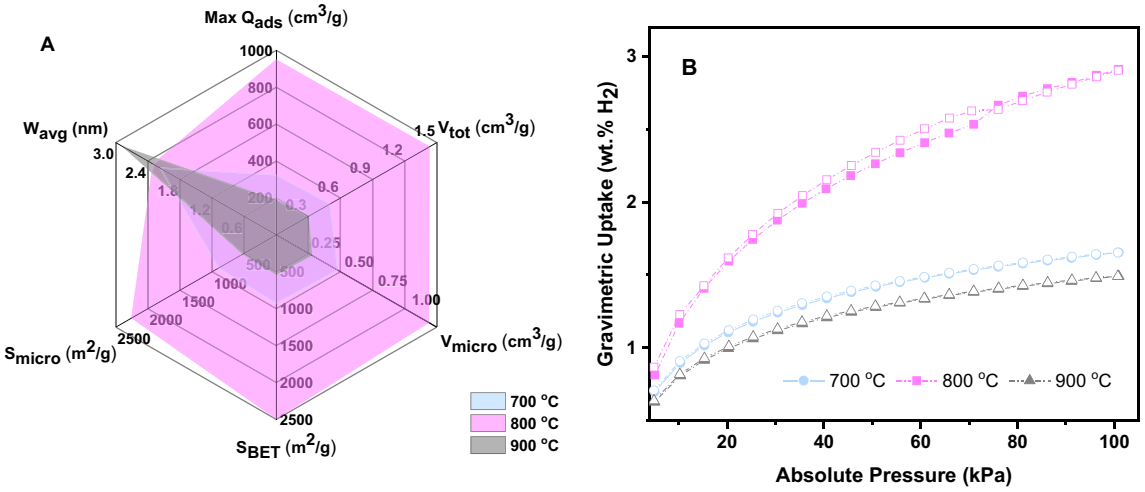

Fig. 1 **A** Radar chart showing the maximum nitrogen adsorbed (Max Q_{ads}), total pore volume (V_{tot}), micropore pore volume (V_{micro}), BET surface area (S_{BET}), micropore surface area (S_{micro}), and pore size (W_{avg}) of activated carbons synthesized at 700 °C (Exp. 2), 800 °C (Exp. 10), and 900 °C (Exp. 9). **B** Hydrogen isotherms show hydrogen uptake at 77 K up to 100 kPa

induce pore collapse, diminishing the beneficial effects on surface area. The results demonstrate this phenomenon, as shown in Table 3, where an observed reduction in surface area occurs at an activation temperature of 900 °C. Excessive heat during activation can disrupt pore structures, which is undesirable when preparing porous materials [55]. Linares-Solano et al. [56] also reported that temperatures above 800 °C negatively impact reaction yield and narrow pore size distribution. Consistent with the findings of this study, a rise in temperature leads to a drop in yield, mostly because of the increased burn-off of carbon material. A sharp decrease in yield of 16% was obtained at 900 °C. As shown in Table S3 of the supplemental material, yields decreased as temperature increased. This drop was attributed to the increasing carbon burn-off and the volatilization of non-carbon components [57]. The optimal activation temperature, therefore, lies at the intersection of enhanced pore development and potential structural integrity concerns.

3.2.2 Impact of KOH weight ratio on adsorptive properties of synthesized biocarbon

The proportion of precursor material to KOH by weight significantly influences the adsorptive properties of activated carbons. Several studies have investigated using alkaline hydroxides to prepare activated carbons [32, 41, 42, 58, 59]. Activated carbon synthesized using hydroxides stands out for its unique qualities, such as low ash content, narrow pore size distribution, and high adsorption capacity [2, 56]. Table 3 and Fig. 2 present the findings of the conducted analysis on the synthesized biocarbon's textural properties and hydrogen uptake, considering different weight ratios of KOH to precursor ratio at 800 °C.

Table 3 shows that the surface area of the activated biocarbon samples increases when the chemical weight ratio of KOH increases. An increase in the chemical weight ratio leads to a greater extent of the reaction, resulting in an increased surface area. This is mostly owing to the etching effect caused by KOH on the carbon precursor. This results in more adsorption sites and improved accessibility for adsorbates [60]. An increase in the weight ratio from 2 to 3 corresponds to a 68% increase in surface area. Figure 2 shows that a larger weight ratio of chemical reagents results in a greater increase in hydrogen uptake. In the studies conducted by Kwiatkowski et al. [60] and Hassen [61], a similar finding was observed, indicating that an increase in the ratio of KOH impacted both the increase of surface area and the enhancement of adsorption capacity.

Table S3 of the supplementary material shows that an increased KOH weight ratio decreases the activated carbons' yield. As stated, higher KOH ratios typically enhance chemical activation, leading to greater pore development and higher surface areas. However, this also tends to decrease activated carbon yield because more carbon material is consumed in the activation process [62].

3.3 Process of optimization

3.3.1 Statistical analysis

The assessment of model validity was conducted by examining the R^2 parameter, which is measured on a scale of 0 to 1. Higher values are considered more desirable, ideally with a maximum difference of 0.3 [63]. The *F*-value and *P* value are the parameters used to assess the model's significance

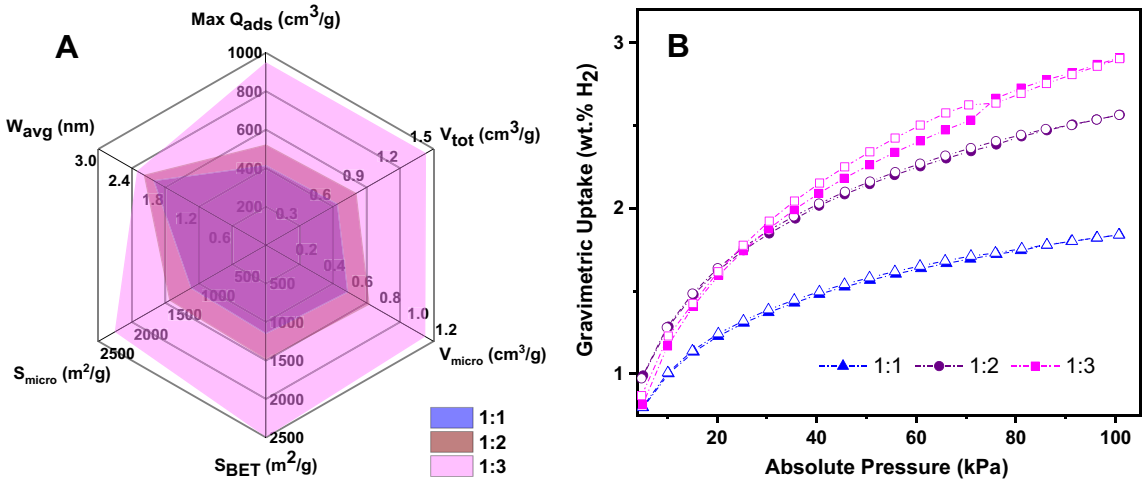

Fig. 2 **A** Radar chart showing the maximum nitrogen adsorbed (Max Q_{ads}), total pore volume (V_{tot}), micropore pore volume (V_{micro}), BET surface area (S_{BET}), micropore surface area (S_{micro}), and pore size (W_{avg}) of activated carbons synthesized at 800 °C and KOH weight ratio of 1:1 (Exp. 1), 1:2 (Exp. 3), and 1:3 (Exp. 10). **B** Hydrogen isotherms show hydrogen uptake at 77 K up to 100 kPa

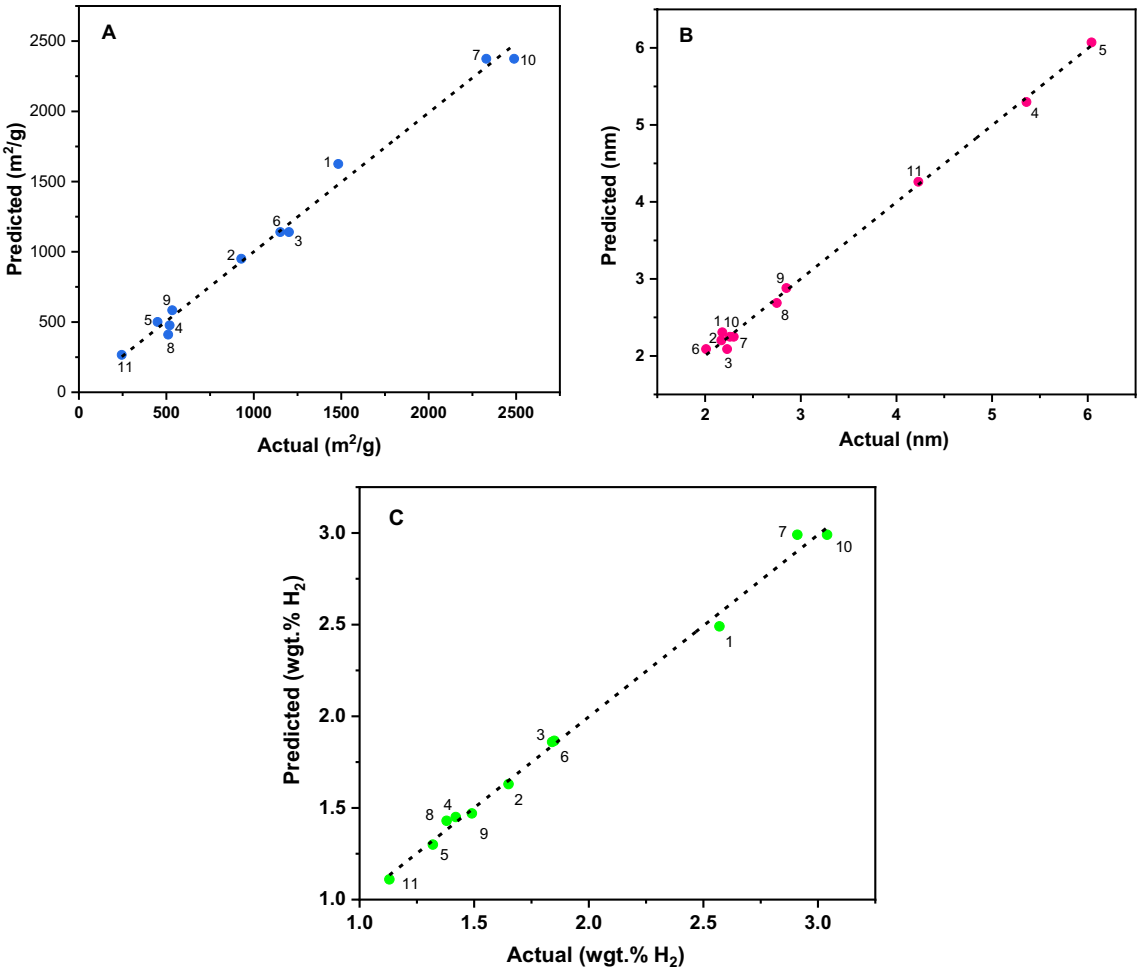

Fig. 3 Experimentally observed points vs model-predicted points (denoted by dotted line) for the three responses: **A** surface area, **B** pore size, and **C** hydrogen uptake at 77 K. Each data point is labeled with its respective experiment number

Table 4 Analysis of variance (ANOVA) of the responses measured for avocado waste-derived activated biocarbons

Response	R^2	Adj. R^2	Pred. R^2	Adeq. Prec	F-value	P value
Surface area	0.990	0.975	0.887	22.11	66.85	0.0006
Pore size	0.997	0.991	0.896	33.92	151.84	0.0008
H_2 uptake	0.995	0.988	0.955	32.58	139.14	0.0001

and fitness. Figure 3 shows the alignment between the predictions made by the model and the experimental outcomes for all responses. Additionally, Table 4 presents the specifics of the ANOVA analysis. For each response, experimental data points exhibit a significant alignment with the model predictions, leading to a high value of R^2.

The R^2 values for the surface area, pore size, and H_2 uptake are 0.990, 0.997, and 0.995, respectively. These values are close to 1 and are considered ideal. The adjusted R^2 values of 0.975, 0.991, and 0.988 demonstrate satisfactory agreement with the predicted R^2 values of 0.887, 0.896, and 0.955 for surface area, pore size, and H_2 uptake, respectively. In order for the Adj. R^2 and Pred. R^2 to be considered quite agreeable, their difference should be below 0.20 [64]. The Adj. R^2 and Pred. R^2 differ by 0.088, 0.095, and 0.033 for surface area, pore size, and H_2 uptake, respectively. Adequate precision is determined by comparing the anticipated values at the design point to the average prediction error. A model is considered acceptable and has adequate precision if its value exceeds 4 [64]. The surface area, pore size, and H_2 uptake values that meet the required precision are 22.11, 33.92, and 32.58, respectively. According to Hou et al. (2013), the F-value and P value are important indicators of a model's statistical

significance and fitness. The *F*-values of 66.85, 151.84, and 139.14 for surface area, pore size, and H_2 uptake, respectively, together with the *P* values of all responses being less than 0.05, indicate that the models effectively align with the experimental data and give a satisfactory fit.

3.3.2 Optimization of preparation parameters

This section examines the optimal parameters for preparing activated carbon to achieve maximum surface area, hydrogen uptake, and smaller pore size necessary for effective hydrogen storage. The optimal preparation conditions were established using the desirability function of Design Expert software to yield the desired outcomes. The surface plot in Fig. 4 depicts desirability while maintaining activation temperature and KOH weight ratio within the studied range.

The optimal conditions derived from numerical optimization for achieving the desired responses of maximizing surface area, hydrogen uptake, and smaller pore size are presented in Table 5. The proposed optimal conditions outlined in Table 5 have a desirability value of 0.957. Validation experiments conducted using these optimal processing conditions resulted in a material with a surface area of 2529.8 m^2/g, a pore size of 2.31 nm, and a hydrogen uptake of 3.07 wt% at 77 K and 1 bar, with predicted and experimental results showing good agreement within an error range of 2–4%. These results validate the predictions of the ANOVA model for the responses under experimental conditions.

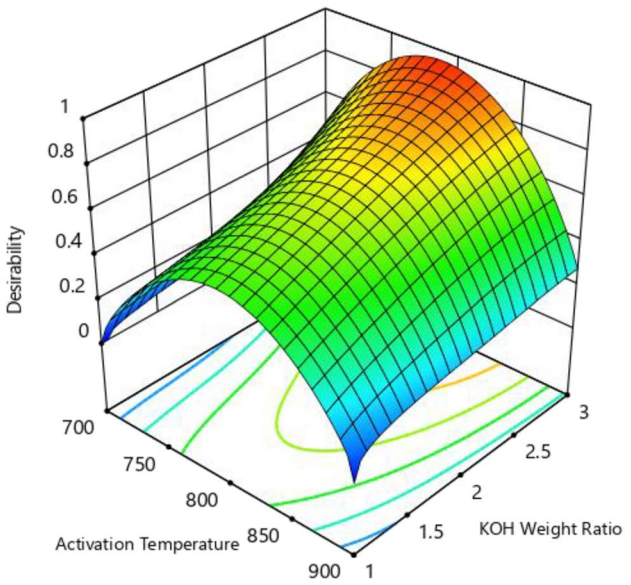

Fig. 4 Three-dimensional surface plots of desirability for numerical optimization of the goal of maximized surface area, hydrogen uptake, and smaller pore size

3.4 Analysis of optimal activated biocarbons

The optimal process parameters were then employed to synthesize activated biocarbons with hydrochars H_{180}, H_{200}, and H_{220} as precursors. These materials' (AC_{180}, AC_{200}, and AC_{220}) physiochemical and adsorptive characteristics were evaluated to assess the impact of hydrothermal pre-treatment temperatures.

3.4.1 Characterizations

The surface morphology of the hydrochars (H_{180}, H_{200}, and H_{220}) and activated biocarbons (AC_{180}, AC_{200}, and AC_{220}) are shown in Fig. 5. The SEM analysis of the hydrochars (depicted in Fig. 5A–C) revealed a surface featuring macro pore formation, indicating the potential of avocado waste hydrothermal pre-treatment to yield a porous carbon material. Subsequent activation of the hydrochars with KOH at high temperatures led to the formation of smaller pores on the material surface, as illustrated in Fig. 5D–F. These images indicate that while the activated materials maintained their original morphology, they underwent size reduction and surface roughening, likely attributed to material decomposition and shrinkage during activation, thus generating additional surface pore structures.

The X-ray diffraction (XRD) spectrum of the optimized activated biocarbon, as shown in Fig. 6A, reveals an identified peak at around $2\theta = 10°$, associated closely with (002) [65]. This peak indicates the existence of an amorphous or disordered carbon structure, typical of biomass-derived activated carbons where the disordered carbonaceous materials contribute to peaks at lower angles [42]. The second identified peak at $2\theta = 35°$ is associated with (100) graphitic planes [66, 67]. This peak indicates some degree of graphitic structure within the optimized activated biocarbons. The analysis of the XRD spectrum indicates that the optimized activated biocarbon derived from avocado waste exhibits a blend of amorphous and graphitic carbon structures. Prior studies have also documented that the carbonization and activation process substantially influences the formation of amorphous carbon and porous architecture [42, 68].

Table 5 Optimum parameters obtained from RSM optimization and model validation

		Surface area (m^2/g)			Pore size (nm)			Hydrogen uptake (%)		
Temp. (°C)	KOH ratio	Pred	Exp	Error (%)	Pred	Exp	Error (%)	Pred	Exp	Error (%)
800	3	2478.7	2529.8	2.06	2.23	2.31	3.6	2.99	3.07	2.6

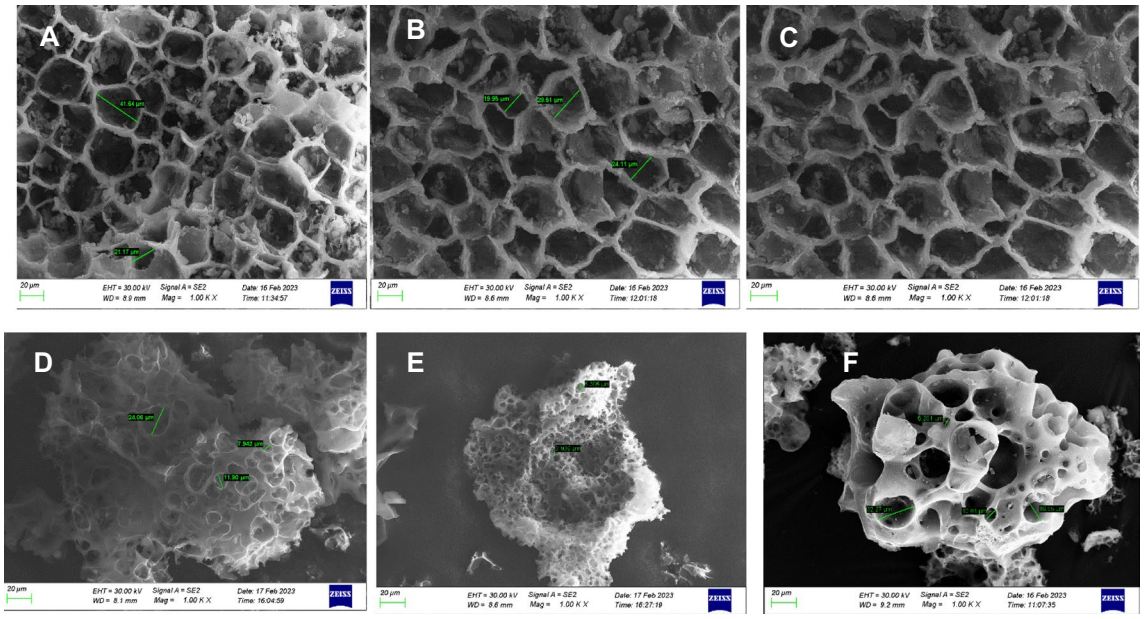

Fig. 5 SEM images of **A** HC_{180}, **B** HC_{200}, **C** HC_{220}, **D** AC_{180}, **E** AC_{200}, and **F** AC_{220}

The Fourier transform infrared (FTIR) spectrum, as shown in Fig. 6B and Fig. S3 in supplementary material, exhibits many distinct peaks, indicating the existence of diverse functional groups. The aliphatic hydrocarbons, most likely derived from the lipid content in the avocado waste, are indicated by the aliphatic C-H stretch at 2882 cm^{-1}. The identification of a C=C stretching vibration at 1631 cm^{-1} indicates the existence of aromatic structures, maybe originating from lignin or other phenolic chemicals present in the waste material. Furthermore, the presence of aromatic structures is further supported by the peak observed at 1492 cm^{-1}, which can be attributed to the stretching vibrations of aromatic C=C bonds. The observation of a peak at 1293 cm^{-1} indicates the C-O stretching vibration, suggesting the existence of oxygen-containing functional groups such as alcohols, ethers, or esters [69]. These functional groups may originate from cellulose or hemicellulose constituents in the avocado waste.

Additionally, the observation of a peak at 1075 cm^{-1} implies the presence of a C-O bond, which may imply the presence of carboxylic acids or esters. These compounds might originate from pectin or other organic acids found in the avocado waste. The FTIR spectrum exhibits a combination of aliphatic and aromatic hydrocarbons and oxygen-containing functional groups commonly found in carbon compounds generated from biomass [42, 69].

Nitrogen (N_2) sorption experiments were conducted to evaluate the optimized biocarbons' specific surface area and porous structure, with pore size distributions (PSDs) analyzed using the non-local density functional theory (NLDFT) model. The N_2 adsorption–desorption isotherm is shown in Fig. 6C, exhibiting a type IV isotherm according to the IUPAC classification [70]. The significant increase before reaching relative pressure P/P_o at 0.4 indicates the presence of micropores in the materials, facilitating increased adsorption at low pressures [71]. When the relative pressure P/P_o exceeds 0.4, the desorption and adsorption isotherms do not overlap, resulting in a hysteresis loop. This loop indicates the presence of mesopores [72]. This clearly illustrates the coexistence of micro- and mesoporous structures within the avocado waste-derived biocarbons. The combination of micropores and mesopores is often most effective for enhanced hydrogen storage in activated carbons. Micropores maximize the surface area available for hydrogen adsorption. At the same time, mesopores facilitate the accessibility of hydrogen molecules to the interior regions of the material. This synergistic effect improves both the adsorption capacity and the kinetics of hydrogen uptake and release [73, 74].

Figure 6D shows the PSDs estimated using the NLDFT model. All three materials showed a bimodal PSD, with the first peak at 0.7–0.8 nm and the second at 2.3 nm in the micropore and mesopore regions. In addition, the three materials exhibited a broad peak at 0.7–0.8 nm and a shoulder around 1–2 nm. The existence of supermicropores (0.7–2 nm) [75] was observed. When the pores are filled with nitrogen, the pore volume diminishes and becomes insignificant beyond the mesopore domain at a pore diameter of around 4–5 nm. The PSD curve revealed the presence of micropores and mesopores, aligning with the nitrogen isotherms' observations. While all three materials have porous structures, including micropores and mesopores,

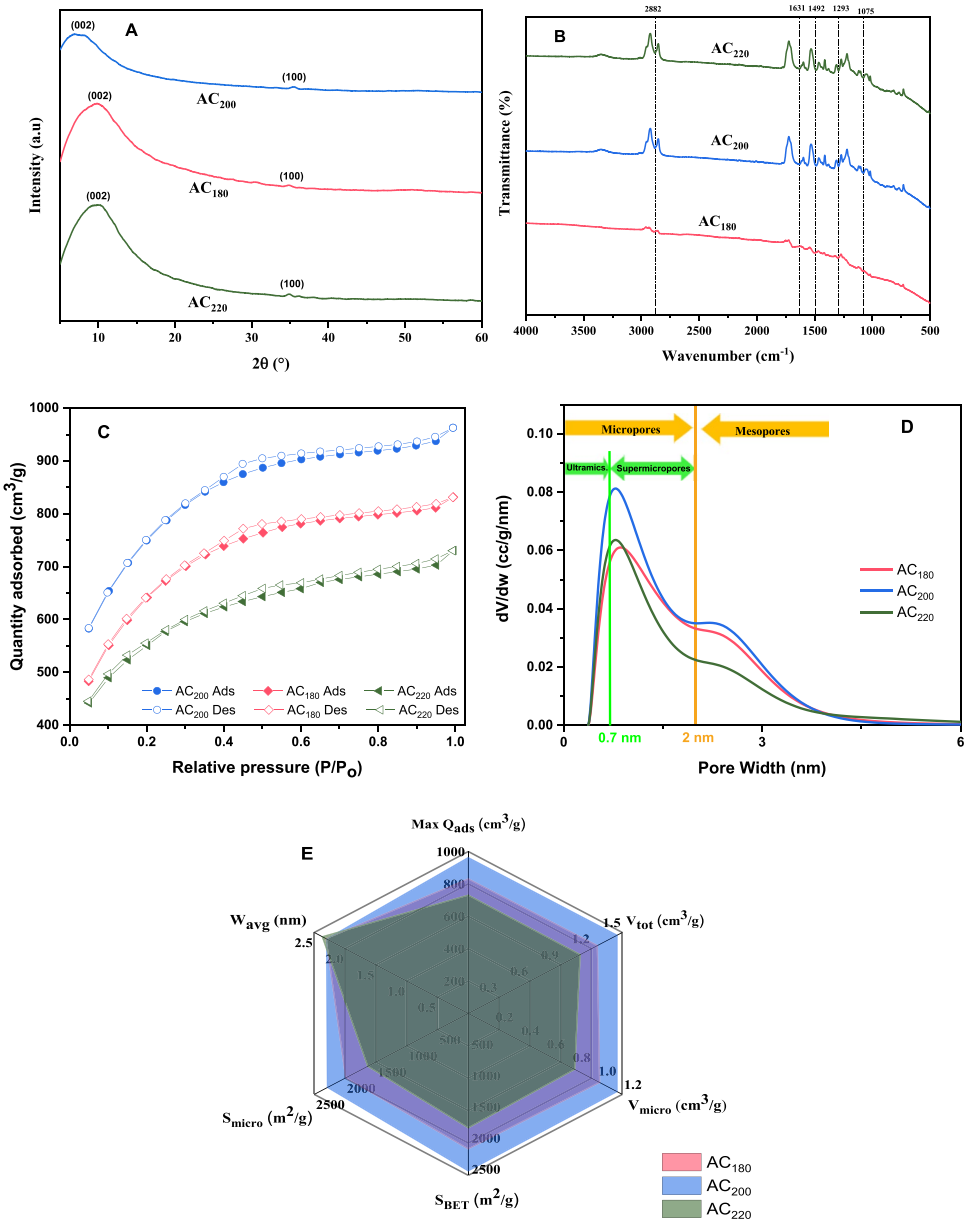

Fig. 6 Characterizations of the optimized activated carbons: **A** XRD pattern; **B** FTIR spectra; **C** N_2 isotherms at 77 K; **D** pore size distribution (PSD) using the NLDFT method; and **E** radar chart showing the maximum quantity of nitrogen adsorbed (Q_{ads}), total pore volume (V_{tot}), micropore volume (V_{micro}), BET surface area (S_{BET}), micropore area (S_{micro}), and average pore diameter

their differences mostly lie in the micropore-to-mesopore volume ratio. This is primarily influenced by different hydrothermal carbonization (HTC) temperatures.

The radar chart in Fig. 6E visually depicts the adsorptive properties of the optimized biocarbons. AC_{200} exhibits the highest surface area (SA) and pore volume (PV) at 2529.8 m^2/g and 1.45 cm^3/g, respectively. In comparison, AC_{180} and AC_{220} show SA and PV of 2178.1 m^2/g and 1.26 cm^3/g and 1838.4 m^2/g and 1.09 cm^3/g, respectively. All biocarbons exhibit a significant degree of microporosity, wherein micropores account for 81.4% (AC_{180}), 80% (AC_{200}), and 76% (AC_{220}) of the total pore volume. The surface area and pore volume increase with rising hydrothermal carbonization (HTC) temperature up to 200 °C but decrease afterward due to intensified decomposition reactions. Higher HTC temperatures promote the breakdown of larger molecules in the precursor material, creating more void spaces and increasing specific surface area, leading to micropores and mesopores [76]. However, excessive heat can collapse the pore wall, reducing surface area and pore volume [77], as observed when HTC temperature surpasses 200 °C. Hence, identifying the optimal HTC temperature is crucial, as it varies depending on the precursor material. This study demonstrates that an HTC temperature of 200 °C for avocado waste yields porous carbon material with enhanced pore characteristics.

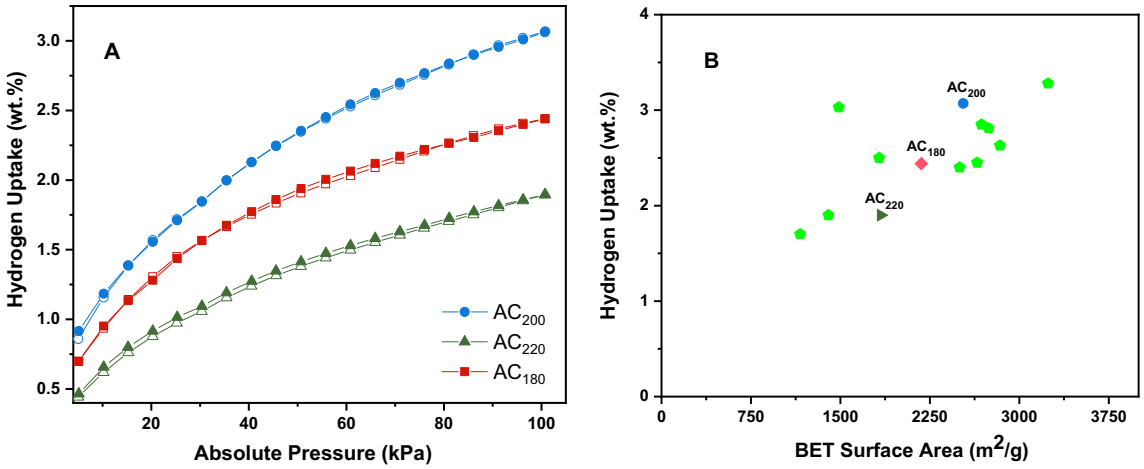

Fig. 7 **A** Hydrogen isotherms, showing uptake at 77 K up to 1 bar in the synthesized optimized biocarbon. **B** Hydrogen uptake plotted against the BET surface area for the optimized biocarbon and biomass-derived carbons reported in literature [4, 41–51]

4 Hydrogen uptake of optimal biocarbons

Figure 7A shows the hydrogen adsorption–desorption isotherms for the optimal biocarbons. The isotherms offer a glimpse into how the pore structure of the synthesized nanoporous materials influences hydrogen storage behavior. The isotherms closely resemble Type I, suggesting that saturation occurs due to forming a hydrogen monolayer, as commonly observed on microporous surfaces [9]. The hydrogen uptake for the three materials consistently rises with increasing pressure. However, it does not reach a distinct plateau because of the low pressure. All isotherms' adsorption and desorption branches exhibit an insignificant presence of hysteresis, suggesting that adsorption is reversible [27]. The synthesized biocarbon demonstrates a hydrogen uptake ranging from 1 to 3% by weight, with biocarbon AC_{200}, hydrothermally pretreated at 200 °C, exhibiting the highest uptake at 3.07 wt%. This is partly attributed to its well-developed micropores, as observed in the PSD. Following AC_{200}, AC_{180} shows an uptake of 2.44 wt% and AC_{220} exhibits an uptake of 1.9 wt%. These values for the optimized biocarbons are comparable to or higher than those previously reported for bio-based carbons in the literature, including bean shells [78], walnut shells [79], *Neolamarckia cadamba* [80], sawdust [81], lignin [27], fungi [82], hemp [83], sucrose [84], corn grain [85], and rice husks [86].

In comparison, commercial activated carbons like MAXSORB MSC-30 and MSP20X have shown hydrogen adsorption capacities of 5.8 wt% and 4.8 wt%, respectively, at 77 K and 40 bar [75], whereas AC_{200} from this work achieved 3.07 wt% at 1 bar, indicating a promising performance at high pressure. Avocado waste-derived activated carbons for hydrogen storage application present a cost-effective and sustainable alternative, offering a novel avenue for biomass valorization and a sustainable and environmentally friendly approach to hydrogen storage. Table S2 in the supplementary material shows the hydrogen adsorption data at 77 K for commercial activated carbons and activated carbons from various biomass feedstocks in the literature to the ACs synthesized in this work.

The improved hydrogen uptake of the optimized biocarbon can be ascribed to its enhanced surface area and significant presence of micropores. This efficiency of narrow micropores is evident in Fig. 7B, where the biocarbons, especially AC_{200} and AC_{180}, outperform materials in the literature with higher surface areas reported by Chen et al. (2838 m^2/g, 2.63 wt%) [78] and Hu et al. (2743 m^2/g, 2.85 wt%) [80]. This highlights the significant role of micropores in enhancing hydrogen uptake. While a higher surface area provides more sites for hydrogen adsorption, micropores facilitate strong van der Waals interactions between hydrogen molecules and the pore walls, enhancing adsorption capacity. The study demonstrates that avocado waste may be transformed into high-value activated biocarbon, resulting in a material with a substantial surface area and significant potential for hydrogen storage.

4.1 Modeling

The universal isotherm model, a type of Monte Carlo simulation developed for sorption modeling, was used to predict the experimental data. This model is also used to calculate the energy of adsorption for each site. The universal isotherm model for three sites, UNIV4, was used. This was also seen as appropriate based on other analyses carried out in terms of hydrogen sorption. The hydrogen heat of vaporization used in this model is 449.36 J/mol. Two terms were used for modeling all activated carbons [44].

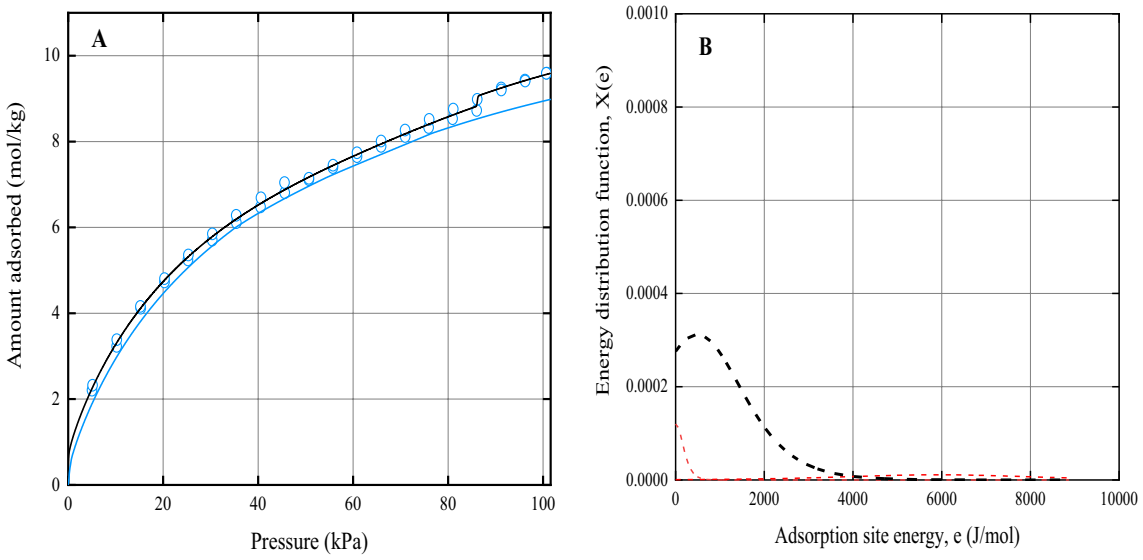

Fig. 8 Predicted and measured data for AC_{180} **A** adsorption isotherm and **B** the corresponding adsorption site energy distribution. The curve with rings in **A** shows the experimental data points, while the blue lines without rings show the universal isotherm model predictions

Figure 8A shows that AC_{180} exhibits Type-IV isotherm. This isotherm is characterized by a rapid increase in the amount of hydrogen adsorbed between 0 and about 86 kPa as the pressure increases, with almost two saturation points or levels being reached. The first pseudo-saturation would be observed between 60 and 80 kPa. After that, we can see a rapid rise or shift in adsorption at pressures above 85 kPa. This shows the multi-layer formation during adsorption at this pressure for AC_{180}. Due to the pressure used in this analysis, we cannot see the actual saturation points. This indicates a well-developed porosity if the pores can still adsorb so much hydrogen at such pressures. Only a fraction of the mesopores seem evident here, and most adsorption occurs in the micropores. The curve with rings shows the experimental data points. In contrast, the blue lines without rings show the predictions of the universal isotherm model.

The energy distribution function, Fig. 8B, shows a non-symmetrical single peak, which is something only seen in type-IV adsorption [44]. Most surface coverage occurs at low pressures, with this region having the highest probability distribution of energy sites. It is also clear that these sites do not require much energy for hydrogen sorption, requiring less than 2000 J/mol for most of the gas sorption and slightly above 300–400 J/mol, which are the most dominant energy site requirements. The apparent mesoporous layer in the multi-layer formation does not require much adsorption energy. It does not have a significant energy site distribution. This could indicate that these are not true mesopores but micropores with higher pore widths, as seen in the PSD.

Figure 9A shows that AC_{200} exhibits Type-V isotherm. This isotherm has a unique S-shape. Three different uptake rates characterize it. There is a smooth uptake at low pressures, between 0 and about 10 kPa, followed by a rapid vertical increase in the amount of hydrogen adsorbed at 10 kPa and a subsequent steep increase of adsorption with increasing pressure, though not as steep as at 10 kPa. This subsequent uptake then levels off at higher pressures, but we cannot see saturation due to the pressures used in this research. This also indicates a well-developed porosity if the pores can adsorb so much hydrogen at such pressures.

Figure 9B shows a Type-V characteristic energy distribution function with a higher probability peak of the energy distribution function at lower energy sites, indicating that most surface coverage occurs at lower concentrations [44]. It is also interesting to note that there are two apparent peaks, with the last peak showing a very small probability of energy sites, though an important amount of adsorption site energy of about 25 000 J/mol at higher pressures.

Figure 10A shows that AC_{220} exhibits Type-IV isotherm, similar to AC_{180}. There is a rapid increase in the amount of hydrogen adsorbed between 0 and about 77 kPa as the pressure increases, with almost two saturation points or levels being reached. The first pseudo-saturation would be observed between 60 and 78 kPa. After that, we can see a rapid rise in adsorption at pressures above 82 kPa. This shows the multi-layer formation during adsorption at this pressure for AC_{220}. This indicates a well-developed porosity with only a fraction of the mesoporous layer contributing to hydrogen adsorption; most adsorption occurs at the micropores. It could also indicate wider micropores and not a real mesoporous layer.

The energy distribution function in Fig. 10B shows a rather interesting non-symmetrical peak at the distribution's

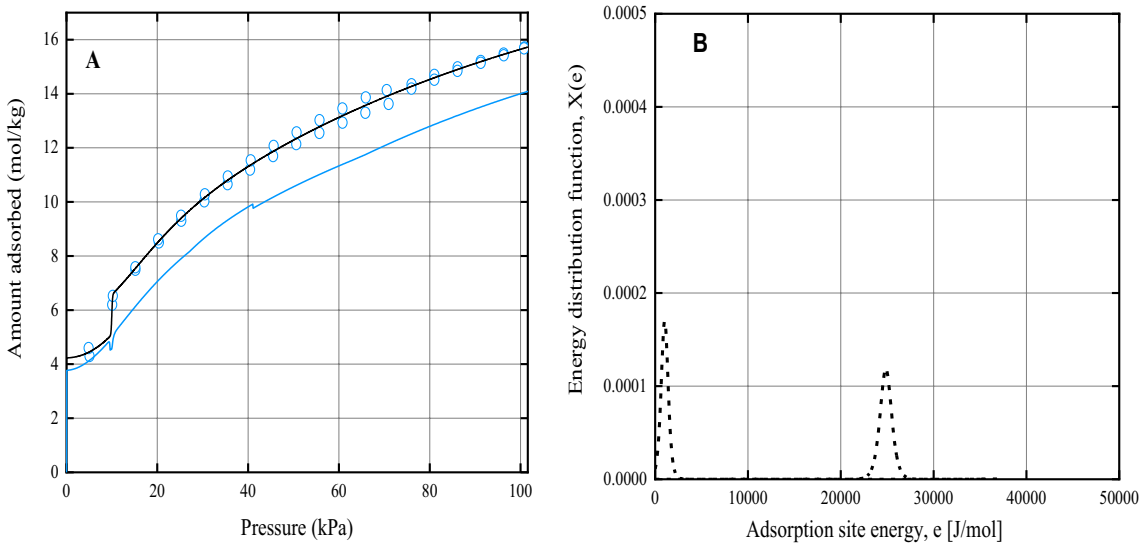

Fig. 9 Predicted and measured data for AC_{200} **A** adsorption isotherm and **B** the corresponding adsorption sites energy distribution. The curve with rings in **A** shows the experimental data points, while the blue lines without rings show the universal isotherm model predictions

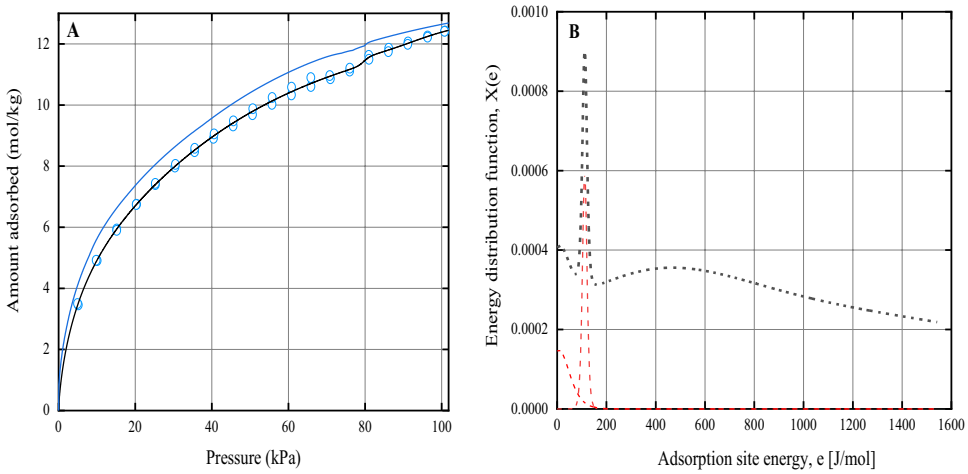

Fig. 10 Predicted and measured data for AC_{220} **A** adsorption isotherm and **B** the corresponding adsorption sites energy distribution. The curve with rings in **A** shows the experimental data points, while the blue lines without rings show the universal isotherm model predictions

lower concentration/pressure end. We can see lower adsorption energy sites exist for AC_{220}, ranging between 0 and just over 1800 J/mol. Adsorption happens easily in the lower-pressure region for this material.

Per the discussion under Section 3.4.1, there are a number of functional groups in the activated carbons. The aliphatic C-H is likely a result of the lipid composition in the avocado waste, while the aromatic C = C stretching vibration may be attributed to lignin or other phenolic chemicals. The presence of oxygen-containing functional groups, as indicated by the C-O stretching vibration, suggests the existence of activated carbons with van der Waals interactions with hydrogen and potentially weak hydrogen bonds. As alluded to in the discussions for Figs. 8B, 9B, and 10B, there is a correlation between pore characteristics and energy distribution. Specifically, hydrogen adsorption requires less energy in well-developed micropores because the van der Waals forces/interactions between activated carbons and hydrogen are stronger.

On the other hand, mesopores require a greater amount of energy for the process of adsorption. Additionally, macropores or the bigger mesopores necessitate even more energy as the van der Waals forces weaken due to the increased contact distance. The micropores with well-developed structures exhibit the most prominent distribution of energy sites, primarily because of their substantial surface area to volume ratio. As a result, most adsorption occurs in the micropores, which need less energy for adsorption than the meso- and macropores. As a result, the micropores have a better capacity to adsorb hydrogen at lower pressures due to stronger connections. In contrast, the larger pores require higher pressures for hydrogen adsorption due to weaker contacts.

5 Conclusion

This study utilized the design of experiment methodology to prepare activated carbons from avocado waste, offering valuable insights into their potential for hydrogen storage. Regression analysis identified an activation temperature of 800 °C and a KOH weight ratio of 3 as optimal process conditions for maximizing hydrogen uptake. Validation experiments confirmed close agreement with predicted responses, yielding material with a surface area of 2529.8 m [2]/g, a pore size of 2.31 nm, and a hydrogen uptake of 3.07 wt%.

Additionally, investigation into hydrothermal carbonization temperatures (180 °C, 200 °C, and 220 °C) revealed superior performance of activated carbon derived from 200 °C pre-treatment, showing enhanced surface properties and higher hydrogen adsorption capacity. Notably, activated carbon from 200 °C pre-treatment exhibited the best pore volume at narrower pore widths, resulting in the highest hydrogen uptake of 3.07 wt%. Micropores predominantly characterized the resulting activated carbons, explaining their high hydrogen uptake. In addition, employing energy distribution functions and homotattic patch approximation, the study found that the two-term universal adsorption isotherm model accurately predicted experimental data, shedding light on the adsorption energy sites of synthesized activated carbons. This study demonstrates avocado waste's potential as feedstock for producing high surface area, well-developed porosity-activated carbons for hydrogen storage, holding promise for advancing renewable energy technologies and addressing global energy challenges.

Supplementary Information The online version contains supplementary material available at https://doi.org/10.1007/s13399-024-06006-1.

Acknowledgements The authors thank James Mehl from the South African Avocado Growers Association (SAAGA) and Andre Oosthuisen from Westfalia Fruits for supplying the avocado waste sample. Sincere gratitude to the Carnegie Corporation of New York for granting Dr. Jibril Abdulsalam the Carnegie research fellowship during this study.

Author contribution LM: methodology, data curation, formal analysis, investigation, software, and writing—original draft. JA: conceptualization, formal analysis, software, writing—review and editing, visualization, and supervision. JM: resources, supervision, and project administration. All authors read and approved the final manuscript.

Funding Open access funding provided by University of the Witwatersrand. The corresponding author acknowledges the funding support from the Carnegie Corporation of New York.

Data availability All data generated or analyzed during this study are included in this published article.

Declarations

Ethics approval and consent to participate Not applicable.

Consent for publication Not applicable.

Competing interests The authors declare no competing interests.

References

1. Oyedepo SO (2012) On energy for sustainable development in Nigeria. Renew Sust Energ Rev 16(5):2583–2598
2. Energy Do (2019) The South African energy sector report. Pretoria. 2019 Contract No.: ISBN: 978–1–920435–17–2
3. Marbán G, Valdés-Solís T (2007) Towards the hydrogen economy? Int J Hydrogen Energy 32(12):1625–1637
4. Rahman A, Farrok O, Haque MM (2022) Environmental impact of renewable energy source-based electrical power plants: solar, wind, hydroelectric, biomass, geothermal, tidal, ocean, and osmotic. Renew Sust Energ Rev 161:112279
5. Elyasi S, Saha S, Hameed N, Mahon PJ, Juodkazis S, Salim N (2024) Emerging trends in biomass-derived porous carbon materials for hydrogen storage. Int J Hydrogen Energy 62:272–306
6. Ahmed I, Zia MA, Afzal H, Ahmed S, Ahmad M, Akram Z et al (2021) Socio-economic and environmental impacts of biomass valorisation: a strategic drive for sustainable bioeconomy. Sustainability 13(8):4200
7. Yu X, Tang Z, Sun D, Ouyang L, Zhu M (2017) Recent advances and remaining challenges of nanostructured materials for hydrogen storage applications. Prog Mater Sci 88:1–48
8. Sevilla M, Mokaya R (2014) Energy storage applications of activated carbons: supercapacitors and hydrogen storage. Energy Environ Sci 7(4):1250–1280
9. Zhang C, Geng Z, Cai M, Zhang J, Liu X, Xin H et al (2013) Microstructure regulation of super activated carbon from biomass source corncob with enhanced hydrogen uptake. Int J Hydrogen Energy 38(22):9243–9250
10. Bader N, Ouederni A (2016) Optimization of biomass-based carbon materials for hydrogen storage. J Energy Storage 5:77–84
11. Hu W, Li Y, Zheng M, Xiao Y, Dong H, Liang Y et al (2021) Degradation of biomass components to prepare porous carbon for exceptional hydrogen storage capacity. Int J Hydrogen Energy 46(7):5418–5426
12. Stelitano S, Conte G, Policicchio A, Aloise A, Desiderio G, Agostino RG (2020) Pinecone-derived activated carbons as an effective medium for hydrogen storage. Energies 13(9):2237
13. Ariharan A, Ramesh K, Vinayagamoorthi R, Rani MS, Viswanathan B, Ramaprabhu S et al (2021) Biomass derived phosphorous containing porous carbon material for hydrogen storage and high-performance supercapacitor applications. J Energy Storage 35:102185
14. Lv L, Huang Y, Cao D (2018) Nitrogen-doped porous carbons with ultrahigh specific surface area as bifunctional materials for dye removal of wastewater and supercapacitors. Appl Surf Sci 456:184–194

15. Saha N, Reza MT (2021) Upcycling simulated food wastes into superactivated hydrochar for remarkable hydrogen storage. J Anal Appl Pyrolysis 159:105322
16. Musyoka NM, Mutuma BK, Manyala N (2020) Onion-derived activated carbons with enhanced surface area for improved hydrogen storage and electrochemical energy application. RSC Adv 10(45):26928–26936
17. Samantaray SS, Mangisetti SR, Ramaprabhu S (2019) Investigation of room temperature hydrogen storage in biomass-derived activated carbon. J Alloy Compd 789:800–804
18. Shahbandeh M. (2024) Global avocado production 2000–2022: Statista. [cited 2024]. Available from: https://www.statista.com/statistics/577455/world-avocado-production/
19. FAO. OECD-FAO (2021) agricultural outlook 2021–2030. Available from: https://www.fao.org/3/cb5332en/Other.pdf
20. Leite AB, Saucier C, Lima EC, Dos Reis GS, Umpierres CS, Mello BL et al (2018) Activated carbons from avocado seed: optimisation and application for removal of several emerging organic compounds. Environ Sci Pollut Res 25:7647–7661
21. Molina-Balmaceda A, Rojas-Candia V, Arismendi D, Richter P (2024) Activated carbon from avocado seed as sorbent phase for microextraction technologies: activation, characterization, and analytical performance. Anal Bioanal Chem 416(10):2399–2409
22. Kassahun D, Khalid S, Shimeles A (2016) Kinetic and thermodynamic study of phenol removal from water using activated carbon synthesizes from avocado kernel seed. Int Lett Nat Sci 54:42–57
23. Rodrigues LA, da Silva MLCP, Alvarez-Mendes MO, dos Reis CA, Thim GP (2011) Phenol removal from aqueous solution by activated carbon produced from avocado kernel seeds. Chem Eng J 174(1):49–57
24. Zhu Y, Kolar P, Shah SB, Cheng JJ, Lim P (2016) Avocado seed-derived activated carbon for mitigation of aqueous ammonium. Ind Crops Prod 92:34–41
25. Palma C, Lloret L, Puen A, Tobar M, Contreras E (2016) Production of carbonaceous material from avocado peel for its application as alternative adsorbent for dyes removal. Chin J Chem Eng 24(4):521–528
26. Tefera N, Mulualem Y, Fito J (2020) Adsorption of fluoride from aqueous solution and groundwater onto activated carbon of avocado seeds. Water Conserv Sci Eng 5:187–197
27. Rowlandson JL, OBrien JC, Edler KJ, Tian M, Ting VP (2019) Application of experimental design to hydrogen storage: optimisation of lignin-derived carbons. J Carbon Res 5(4):82
28. Loloie Z, Mozaffarian M, Soleimani M, Asassian N (2017) Carbonization and CO 2 activation of scrap tires: optimization of specific surface area by the Taguchi method. Korean J Chem Eng 34:366–375
29. Sumathi S, Bhatia S, Lee K, Mohamed A (2009) Optimization of microporous palm shell activated carbon production for flue gas desulphurization: experimental and statistical studies. Bioresour Technol 100(4):1614–1621
30. Cheng F, Liang J, Zhao J, Tao Z, Chen J (2008) Biomass waste-derived microporous carbons with controlled texture and enhanced hydrogen uptake. Chem Mater 20(5):1889–1895
31. Khoshraftar Z, Ghaemi A (2022) Presence of activated carbon particles from waste walnut shell as a biosorbent in monoethanolamine (MEA) solution to enhance carbon dioxide absorption. Heliyon. 8(1):e08689
32. Abdulsalam J, Mulopo J, Oboirien B, Bada S, Falcon R (2019) Experimental evaluation of activated carbon derived from South Africa discard coal for natural gas storage. Int J Coal Sci Technol 6(3):459–477
33. Rosli NA, Ahmad MA, Noh TU (2023) Unleashing the potential of pineapple peel-based activated carbon: response surface methodology optimization and regeneration for methylene blue and methyl red dyes adsorption. Inorg Chem Commun 155:111041
34. Xia Y, Yang Z, Zhu Y (2013) Porous carbon-based materials for hydrogen storage: advancement and challenges. J Mater Chem, A 1(33):9365–9381
35. Masika E, Mokaya R (2012) Hydrogen storage in high surface area carbons with identical surface areas but different pore sizes: direct demonstration of the effects of pore size. J Phys Chem C 116(49):25734–25740
36. Blankenship LS, Mokaya R (2022) Modulating the porosity of carbons for improved adsorption of hydrogen, carbon dioxide, and methane: a review. Mater Ad 3(4):1905–1930
37. De Rose E, Bartucci S, Bonaventura CP, Conte G, Agostino RG, Policicchio A (2023) Effects of activation temperature and time on porosity features of activated carbons derived from lemon peel and preliminary hydrogen adsorption tests. Colloids Surf, A. 672:131727
38. Laudisio G, Dash RK, Singer JP, Yushin G, Gogotsi Y, Fischer JE (2006) Carbide-derived carbons: a comparative study of porosity based on small-angle scattering and adsorption isotherms. Langmuir 22(21):8945–8950
39. Leonzio G (2017) Optimization through response surface methodology of a reactor producing methanol by the hydrogenation of carbon dioxide. Processes 5(4):62
40. Montgomery DC (2017) Design and analysis of experiments. John Wiley & Sons
41. Abdulsalam J, Mulopo J, Bada S, Oboirien B (2020) Natural gas storage properties of adsorbents synthesised from three different coal waste in South Africa. Fuel 267:117157
42. Abdulsalam J, Otun K, Gardee N, Patel B, Leswifi T, Mathe MK (2023) Activated biocarbon from paper mill sludge as electrode material for supercapacitors: comparative performance evaluation in two aqueous electrolytes. ACS Omega 8(6):5285–5299
43. Erdogan FO (2019) Freundlich, Langmuir, Temkin, Harkins-Jura isotherms studies of H2 adsorption on porous adsorbents. Chem Chemical Technol. 13(2):129–35
44. Ng KC, Burhan M, Shahzad MW, Ismail AB (2017) A universal isotherm model to capture adsorption uptake and energy distribution of porous heterogeneous surface. Sci Rep 7(1):10634
45. Ioannidou O, Zabaniotou A (2007) Agricultural residues as precursors for activated carbon production—a review. Renew Sust Energ Rev 11(9):1966–2005
46. Manyà JJ (2012) Pyrolysis for biochar purposes: a review to establish current knowledge gaps and research needs. Environ Sci Technol 46(15):7939–7954
47. Marsh H, Reinonso- Rodriguez F (2006) Activated carbon Elsevier Science & Technology Books. Elsevier, Amsterdam
48. Bressani R, Rodas B, Ruiz A (2009) La composición química, capacidad antioxidativa y valor nutritivo de la semilla de variedades de aguacate. Fondo Nacional de Ciencia y Tecnología-FONACYT, Universidad del Valle de Guatemala-UVG, Tegucigalpa (Guatemala)
49. Demirbaş A (2001) Biomass resource facilities and biomass conversion processing for fuels and chemicals. Energy Convers Manage 42(11):1357–1378
50. Islam MT, Sultana AI, Chambers C, Saha S, Saha N, Kirtania K et al (2022) Recent progress on emerging applications of hydrochar. Energies 15(24):9340
51. Vijeata A, Chaudhary GR, Chaudhary S, Ibrahim AA, Umar A (2024) Recent advancements and prospects in carbon-based nanomaterials derived from biomass for environmental remediation applications. Chemosphere 375:141935
52. Liang Q, Liu Y, Chen M, Ma L, Yang B, Li L et al (2020) Optimized preparation of activated carbon from coconut shell and municipal sludge. Mater Chem Phys 241:122327

53. Chen D, Chen X, Sun J, Zheng Z, Fu K (2016) Pyrolysis polygeneration of pine nutshell: quality of pyrolysis products and study on the preparation of activated carbon from biochar. Bioresour Technol 216:629–636
54. Wang J, Nie P, Ding B, Dong S, Hao X, Dou H et al (2017) Biomass-derived carbon for energy storage devices. J Mater Chem, A 5(6):2411–2428
55. Ahmadpour A, Do D (1997) The preparation of activated carbon from macadamia nutshell by chemical activation. Carbon 35(12):1723–1732
56. Linares-Solano A, Lillo-Ródenas M, Marco-Lozar JP, Kunowsky M, Romero-Anaya AJ (2012) NaOH and KOH for preparing activated carbons used in energy and environmental applications. Int J Energy Environ Econ 20(4):355
57. Gao Y, Yue Q, Gao B, Li A (2020) Insight into activated carbon from different kinds of chemical activating agents: a review. Sci Total Environ 746:141094
58. Bardhan M, Novera TM, Tabassum M, Islam MA, Jawad AH, Islam MA (2020) Adsorption of methylene blue onto betel nut husk-based activated carbon prepared by sodium hydroxide activation process. Water Sci Technol 82(9):1932–1949
59. Borghei SA, Zare MH, Ahmadi M, Sadeghi MH, Marjani A, Shirazian S et al (2021) Synthesis of multi-application activated carbon from oak seeds by KOH activation for methylene blue adsorption and electrochemical supercapacitor electrode. Arab J Chem 14(2):102958
60. Kwiatkowski M, Broniek E, Fierro V, Celzard A (2021) An evaluation of the impact of the amount of potassium hydroxide on the porous structure development of activated carbons. Materials 14(8):2045
61. Hassen JH (2017) Effect of KOH ratio on the formation of activated carbon from pressed wood residues. Int J Pharm Sci Res 8(11):4875–4880
62. Li Z, Gao X, Wu L, Wang K, Kobayashi N (2017) Preparation of activated carbons from poplar wood by chemical activation with KOH. J Porous Mater 24:193–202
63. Eriksson L, Johansson E, Kettaneh-Wold N, Wikström C, Wold S (2000) Design of experiments Principles and Applications, Learn Ways AB, Stockholm. Wiley
64. Kraber S (2013) How to get started with Design Expert Software. Stat-Ease, Inc.
65. An Y, Tian Y, Li Y, Wei C, Tao Y, Liu Y et al (2020) Heteroatom-doped 3D porous carbon architectures for highly stable aqueous zinc metal batteries and non-aqueous lithium metal batteries. Chem Eng J 400:125843
66. Boujibar O, Ghosh A, Achak O, Chafik T, Ghamouss F (2019) A high energy storage supercapacitor based on nanoporous activated carbon electrode made from Argan shells with excellent ion transport in aqueous and non-aqueous electrolytes. J Energy Storage 26:100958
67. Yoshizawa N, Maruyama K, Yamada Y, Ishikawa E, Kobayashi M, Toda Y et al (2002) XRD evaluation of KOH activation process and influence of coal rank. Fuel 81(13):1717–1722
68. Zhao Y, Ran W, He J, Song Y, Zhang C, Xiong D-B et al (2015) Oxygen-rich hierarchical porous carbon derived from artemia cyst shells with superior electrochemical performance. ACS Appl Mater Interfaces 7(2):1132–1139
69. Nagalakshmi T, Emmanuel K, Suresh Babu C, Chakrapani C, Divakar PP (2015) Preparation of mesoporous activated carbon from jackfruit PPI-1 waste and development of different surface functional groups. Int Lett Chem Phys Astron 54:189–200
70. Thommes M, Kaneko K, Neimark AV, Olivier JP, Rodriguez-Reinoso F, Rouquerol J et al (2015) Physisorption of gases, with special reference to the evaluation of surface area and pore size distribution (IUPAC Technical Report). Pure Appl Chem 87(9–10):1051–1069
71. Fu S, Fang Q, Li A, Li Z, Han J, Dang X et al (2021) Accurate characterization of full pore size distribution of tight sandstones by low-temperature nitrogen gas adsorption and high-pressure mercury intrusion combination method. Energy Sci Eng 9(1):80–100
72. Hu Z, Srinivasan MP, Ni Y (2000) Preparation of mesoporous high-surface-area activated carbon. Adv Mater 12(1):62–65
73. Fomkin A, Pribylov A, Men'shchikov I, Shkolin A, Aksyutin O, Ishkov A et al (2021) Adsorption-based hydrogen storage in activated carbons and model carbon structures. Reactions. 2(3):209–26
74. Gotzias A, Tylianakis E, Froudakis G, Steriotis T (2012) Theoretical study of hydrogen adsorption in oxygen functionalized carbon slit pores. Microporous Mesoporous Mater 154:38–44
75. Sdanghi G, Schaefer S, Maranzana G, Celzard A, Fierro V (2020) Application of the modified Dubinin-Astakhov equation for a better understanding of high-pressure hydrogen adsorption on activated carbons. Int J Hydrogen Energy 45(48):25912–25926
76. Kozyatnyk I, Benavente V, Weidemann E, Gentili FG, Jansson S (2023) Influence of hydrothermal carbonization conditions on the porosity, functionality, and sorption properties of microalgae hydrochars. Sci Rep 13(1):8562
77. Xiao L-P, Shi Z-J, Xu F, Sun R-C (2012) Hydrothermal carbonization of lignocellulosic biomass. Bioresour Technol 118:619–623
78. Chen T, Zhou Y, Luo L, Wu X, Li Z, Fan M et al (2019) Preparation and characterization of heteroatom self-doped activated biocarbons as hydrogen storage and supercapacitor electrode materials. Electrochim Acta 325:134941
79. Lionetti V, Bonaventura CP, Conte G, De Luca O, Policicchio A, Caruso T et al (2024) Production and physical-chemical characterization of walnut shell-derived activated carbons for hydrogen storage application. Int J Hydrogen Energy 61:639–649
80. Hu W, Huang J, Yu P, Zheng M, Xiao Y, Dong H et al (2019) Hierarchically porous carbon derived from Neolamarckia cadamba for electrochemical capacitance and hydrogen storage. ACS Sustain Chem Eng 7(18):15385–15393
81. Liang Y, Wang Y, Ding N, Liang L, Zhao S, Yin D et al (2023) Preparation and hydrogen storage performance of poplar sawdust biochar with high specific surface area. Ind Crops Prod 200:116788
82. Wang J, Senkovska I, Kaskel S, Liu Q (2014) Chemically activated fungi-based porous carbons for hydrogen storage. Carbon 75:372–380
83. Yang R, Liu G, Li M, Zhang J, Hao X (2012) Preparation and N_2, CO_2 and H_2 adsorption of super activated carbon derived from biomass source hemp (Cannabis sativa L.) stem. Microporous Mesoporous Mater 158:108–16
84. Armandi M, Bonelli B, Geobaldo F, Garrone E (2010) Nanoporous carbon materials obtained by sucrose carbonization in the presence of KOH. Microporous Mesoporous Mater 132(3):414–420
85. Balathanigaimani M, Shim W-G, Kim T-H, Cho S-J, Lee J-W, Moon H (2009) Hydrogen storage on highly porous novel corn grain-based carbon monoliths. Catal Today 146(1–2):234–240
86. Heo Y-J, Park S-J (2015) Synthesis of activated carbon derived from rice husks for improving hydrogen storage capacity. J Ind Eng Chem 31:330–334